Nucleation and initial growth in the semimetallic homoepitaxial system of Bi on Bi(111)

G. Jnawali,[*,†] Th. Wagner,[*,‡] H. Hattab, R. Möller, and M. Horn-von Hoegen
Department of Physics and Center for Nanointegration Duisburg Essen (CeNIDE), University of Duisburg-Essen, Lotharstraße 1, 47057 Duisburg, Germany

(Received 25 November 2008; revised manuscript received 13 March 2009; published 11 May 2009)

The nucleation and initial growth of the semimetallic homoepitaxial system of Bi(111) was studied at 130 K by scanning tunneling microscopy. The island density increases with the cubic root of coverage, i.e., $n_x \propto \Theta^{1/3}$, up to 5.5×10^{11} islands/cm^2 at 0.23 bilayer (BL) coverage. We determined a surface diffusion coefficient of $D=2.6\times10^6$ s^{-1}. Additionally, a transition of the island shape from compact to quasifractal was observed at about 0.1 BL coverage. The transition island size was estimated to be 70 nm^2.

DOI: 10.1103/PhysRevB.79.193306 PACS number(s): 68.55.A−, 68.37.Ef, 68.35.Fx

Crystalline Bi films exhibit a great potential for application in future spintronic devices due to some intriguing properties such as large magnetoresistance effect,[1] highly metallic surface states,[2–5] Rashba-type strong spin-orbit splitting,[2,6] etc. These properties are inherently related to the anomalous electronic behavior of Bi such as low effective mass, low carrier concentration, and large Fermi wavelength ($\lambda_F \sim 30$ nm).[7] An understanding of the origin of these properties requires a detailed structural and morphological characterization of the system.

Surprisingly Bi—as a covalently bonded semimetal—grows in a bilayer-by-bilayer fashion even at temperatures as low as 80 K.[8] The slow builtup of surface roughness due to a weak step edge barrier can be avoided by growth at higher temperatures, i.e., 300–450 K. Then atomically flat layers with very low defect density can be grown. This is also possible for Bi heteroepitaxy on substrates such as Si.[9–11] In order to understand the underlying mechanism, it is essential to study microscopic processes at the early stages of growth. Relevant parameters, which control or govern the growth mechanism, include the surface diffusion coefficient D, the terrace diffusion barrier E_d, and the attempt frequency ν_0 at kinetically limiting conditions (low temperatures). With the knowledge of these fundamental parameters, which depend on the system (both growing material and the substrate), it is also possible to manipulate and control the morphology of the growing film to obtain desired properties.[12]

Here we report on a scanning tunneling microscope (STM) study of initial stages of growth in a semimetallic homoepitaxial system: Bi on Bi(111). From the variation in island density and size in a sub-bilayer regime of coverage, we determine relevant diffusion parameters. The results are discussed in terms of well-established nucleation theory and compared with the parameters for other metallic systems.

The experiments were performed in an ultrahigh vacuum (UHV) system that consists of a main chamber for sample preparation and an analysis chamber, which is equipped with a variable-temperature STM and a conventional low-energy electron diffraction (LEED) system. Bi (purity 99.9999%) was evaporated at room temperature (RT) from a resistively heated ceramic crucible mounted in a water-cooled copper shroud at a deposition rate of 0.01 bilayer (BL)/s [1 BL corresponds to the Bi(111) atomic density of 1.14×10^{15} atoms/cm^2]. The rate was monitored via a quartz microbalance mounted on the evaporator. The background pressure was better than 1×10^{-9} mbar during deposition. High-quality Bi(111) buffer films with a thickness of 20 nm were prepared on Si(111)-(7×7) at RT following a recipe given by Nagao *et al.*[10,11] and Kammler *et al.*[13] and serve as virtual Bi(111) substrates. The (111) orientation of the Bi films was confirmed by LEED. The Bi(111) buffer films are atomically smooth without defects and only exhibit some bilayer high steps at a separation of approximately 100 nm, which does not affect the nucleation behavior during further sub-bilayer deposition of Bi. These Bi buffer films were *in situ* transferred to the analysis chamber and cooled to 130 K. Further Bi deposition in the sub-bilayer regime was performed inside the analysis chamber, employing a second Bi evaporator at a flux of 4×10^{-4} BL/s and a base pressure of 5×10^{-10} mbar. The second Bi source is located at the base flange of the STM and there is a direct flow path between the aperture of the evaporator and the sample if the tip is retracted a few millimeters. This special experimental setup allows us to deposit very low coverage of Bi and subsequently image the topography by STM without major displacements of the sample and changes in the sample temperature.

In order to study the island nucleation and growth we have followed the evolution of Bi(111) surface morphology as a function of coverage at 130 K. Figure 1 shows a series of STM micrographs with a size of (150×150) nm^2 for coverages starting as low as 0.0023 BL up to 0.23 BL of Bi. The micrographs were recorded from two experimental runs under the same conditions. At very low coverage Bi islands are imaged as bright protrusions while at higher coverages irregular shaped islands are apparent. It is also obvious that the island density and the size have increased as functions of coverage [see Figs. 1(a)–1(h)]. Up to the coverage of 0.1 BL, there are exclusively small islands with compact shape. Additionally, a shape transition of the Bi islands is observed around 0.1 BL, where the compact shape of islands is transformed into a quasifractal form. However, no sharp or abrupt transition occurs, as evident from the images in Figs. 1(f)–1(h), where only few of the compact islands have turned into quasifractal shape at 0.115 BL before leading to the anisotropic branching at 0.23 BL.

The island density as a function of Bi coverage was determined from the series of STM micrographs shown in Fig. 1 and plotted in Fig. 2. The island density does not change in the time between the deposition steps as confirmed

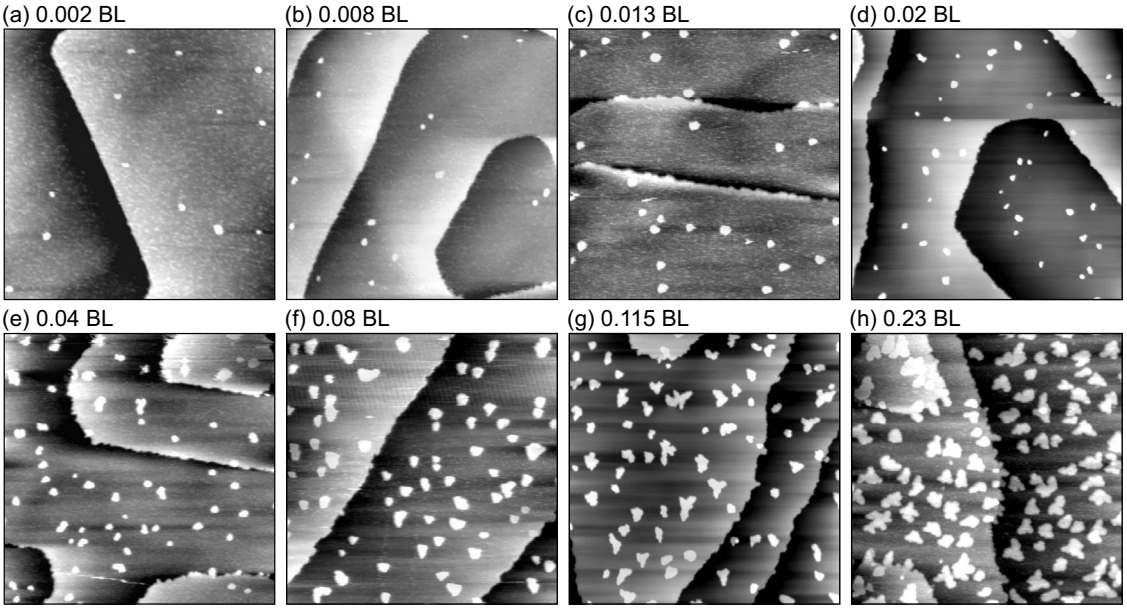

FIG. 1. STM images (image size: (150×150) nm^2, tunneling parameters: $I_{\text{tunnel}}=5-50$ pA and $U_{\text{bias}}=1.0-1.1$ V) showing the variation in island density and the island shape transition from compact to quasifractal shape for different coverages of Bi on a Bi(111) virtual substrate at 130 K. The images are recorded from two experimental runs, i.e., (a), (c), (e), (f), and (h) are from run I and (b), (d), and (g) are from run II. A flux of $R=4\times10^{-4}$ BL/s was used during each deposition for both experimental runs. All images are recorded by applying the bias voltage to the sample with respect to the tip.

by a high-resolution LEED study where the onset of Ostwald ripening was observed only for temperatures above 200 K.[14] Below 200 K the island morphology is stable. The quantitative evaluation of the island density for each coverage was performed by island counting in each STM image. Because denuded zone effects are visible at step edges in the STM micrographs for higher coverages, we have corrected the island density by subtracting the denuded zone area which is proportional to the length of the apparent step edges. The density of islands was normalized to the atomic density of Bi(111) BL to extract the density in terms of atoms per lattice site, equivalent to BL.

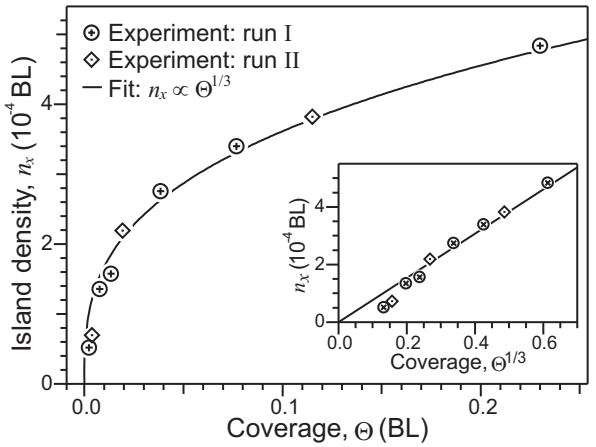

FIG. 2. Island density versus coverage at 130 K, as estimated from the STM images shown in Fig. 1. The data are taken from two experimental runs, i.e., runs I and II. In the inset the data are plotted as a function of the cubic root of Bi coverage, showing a small deviation of island density at very low coverage.

Before we start with the discussion of these results let us briefly recapitulate some of the basics of nucleation theory. A single adatom diffusion on the surface is governed by the diffusion barrier E_d and the attempt frequency ν_0. Both parameters define the migration of the adatom as a random walker on the surface lattice. For two-dimensional (2D) diffusion on a hexagonal lattice, the diffusion coefficient D (in unit cells per second, i.e., s^{-1}) could be expressed by E_d and ν_0 as[15,16]

$$D = \frac{1}{6}\nu_0 \exp\left(\frac{-E_d}{k_B T}\right) = D_0 \exp\left(\frac{-E_d}{k_B T}\right) \tag{1}$$

with $D_0=\frac{1}{6}\nu_0$, known as the prefactor of the diffusion coefficient D, and the substrate temperature T. During the initial phase of deposition the surface diffusion coefficient D determines the outcome of the competition between nucleation of new islands and the coarsening of existing islands. It therefore determines the stable island density at a given deposition rate R. Thus, the value of the diffusion coefficient gives an estimation for the probability that a deposited adatom finds an existing island before it meets with another adatom and forms a stable nucleus and subsequently affects the number density of saturated islands. The saturation island density could be used to calculate the diffusion barrier applying Venables nucleation theory.[17,18] From the Arrhenius plot of the island density versus inverse of deposition temperature for a given sub-bilayer coverage, the terrace diffusion barrier is derived. This approach was successfully applied in a previous high-resolution LEED analysis and an activation barrier of $E_d=0.135$ eV for an adatom diffusion in Bi(111) surface was determined.[8] Here a simple approach is used to relate the island density with coverage for a constant deposition tem-

perature of 130 K and a diffusion coefficient D is extracted.

Dimensional arguments, based on the theory of random walk, applied to the diffusive motion of adatoms in the nucleation process provides a simple relation between the surface adatom diffusion coefficient and the island number density as[19,20]

$$n_x^3 = \frac{3R\Theta}{D}. \quad (2)$$

Equation (2) is valid for long hop distances in an isotropic 2D random-walk system. Additionally, some important assumptions such as the absence of coalescence or coarsening effects must be made before applying Eq. (2), which include mainly: (a) a collision of two adatoms forms a stable dimer and (b) there is no coarsening or coalescence of islands during deposition. Since experiments have been performed at 130 K and Bi atoms are covalently bonded within the lattice,[10] the first assumption is valid for our system. The coverage regime we have studied is far below the coalescence regime, since a previous study exhibited no coalescence at 0.5 BL coverage.[8] Thus, the second assumption also holds true.

According to Eq. (2), we concentrate on the estimation of the island density n_x for different coverages deposited with a constant flux R at 130 K. Figure 2 shows the behavior of island density as a function of coverage. At extremely low coverage regime, the island density increases rapidly because the probability for island nucleation via the formation of a critical nucleus is strongly enhanced with raising adatom density. As the coverage increases, it slows down significantly because exclusive growth of islands becomes dominant. However, no saturation or decrease in the density is apparent in the plot, indicating the absence of coalescence. The experimental data were fitted by using Eq. (2) (see Fig. 2), which agree quite well except for a slight deviation at the very beginning, which is plotted in the inset of Fig. 2. This deviation might be due to the fact that, in the nucleation regime below 0.01 BL, the monomer density is increased compared with the steady-state regime. Since the STM can hardly detect a mobile diffusing Bi adatom, obviously the measured density turns out to be slightly lower than the expected value. An estimate (upper limit) for the average island size is calculated from the ratio of the coverage to the island density at 0.0023 BL and is ~50 atoms, i.e., the experimental observation of the pure nucleation regime is not possible. From the slope of the fit in Fig. 2 the surface diffusion coefficient was estimated to be $D=2.6\times10^6$ s^{-1}. Substituting the value of D and using the diffusion energy of $E_d=0.135$ eV from the previous findings[8] in Eq. (1), the attempt frequency was extracted to be $\nu_0=2.7\times10^{12}$ s^{-1}. This value is quite reasonable in the case of Bi, which has a sufficiently low atomic vibration frequency (bulk phonon frequency of $\nu_0\simeq3\times10^{12}$ s^{-1} for the optical branch[21]) as compared to other metallic systems.

In the following we will describe the island shape transition, which has been observed in the STM analysis. For the quantitative investigation, we determined the perimeter p_i and the area A_i of each individual island from all STM micrographs shown in Fig. 2. All these data pairs (island area A_i and perimeter p_i) are plotted in Fig. 3 where the different symbols represent different deposited coverages. Most of the data points overlap with a curve, which is well described by a square root of the area. This dependence is easily explained for compact islands of the same shape where the perimeter p_i increases, by definition, with increasing the surface area a_i, following the square-root behavior (for circular islands $A_i=p_i^2/4\pi$ and for hexagonal islands $A_i=\sqrt{3}p_i^2/24$). This agrees quite well up to the coverage of 0.08 BL, as shown by the solid line fit in Fig. 3. However, as the coverage is increased to 0.115 BL, some of the islands do appear to be slightly ramified as visible in Fig. 2(g), which causes a deviation from the square-root dependence. At 0.23 BL, almost all of the islands grow in a quasifractal shape, showing a larger perimeter as obvious from the data points which lie far above the solid line of square-root behavior of compact islands. From this deviation in the plot, as indicated by the dotted rectangles with gray background in Fig. 3, the transition size of the islands was estimated to be ~70 nm^2.

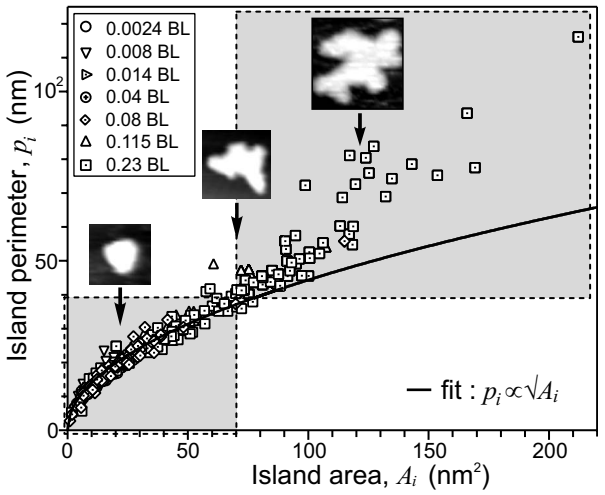

FIG. 3. Island perimeter p_i versus surface area A_i plotted for different coverages, as indicated by different symbols. The solid line represents a square-root fit, i.e., $p_i \propto \sqrt{A_i}$. The critical island size was estimated to be ~70 nm^2. Typical islands from Figs. 1(f)–1(h) are also attached to show the shape transition. All three images are shown in the same magnification scales. The positions of the images within the graph indicate the mean size of the island for the particular coverages. Dotted rectangles with gray background are shown as a guide for the eyes to distinguish the island shape transition regions.

Considering the deposition conditions and the coverage, such a shape transition has rarely been found in other systems. Brune *et al.*[22] observed anisotropic branching of the islands in Ag/Pt(111) beyond the critical island size of heptamer, leading to an exclusive island growth. It has been argued as a low-perimeter mobility for attaching adatoms.[23–25] Unlike this case, the transition island size in our system is quite large, i.e., 70 nm^2 (~800 atoms) and the shape transitions appears at surprisingly high coverage; however, the transformed island shape is quite similar, i.e., branching in the triangular symmetry. This fact obviously reveals that the same argument may hold to the shape transition; however, slightly lower diffusion barrier may have

caused the large critical island size. Brune *et al.*[22] found a value of 0.157 eV for Ag on Pt(111), while in the case of Bi on Bi(111) it is 0.135 eV.[8] Additionally, the shape transition occurred in our case is far from the nucleation regime, i.e., at the steady-state regime, which was not the case for Ag/Pt(111), where the shape transition was found just above the nucleation regime.

In conclusion, epitaxial growth in the semimetallic system of Bi on Bi(111) is well described by the existing diffusion and nucleation theory. The island density increases by $\Theta^{1/3}$ with a transition from compact to fractal shape at the onset of steady-state regime at 0.1 BL coverage. This is in contrast to other metallic systems such as Pt/Pt(111) and Ag/Pt(111),[22,25] where such a shape transition occurs at the transition regime of nucleation and growth, i.e., ~0.01 ML coverage. However, the symmetry of the quasifractal islands after the shape transition matches for both cases, i.e., threefold symmetry. This originates from the threefold symmetry of the (111) surface. In spite of its directional covalent bonds, Bi exhibits a nucleation and growth characteristics, which are more typical for a metallic system.

Financial support from the Deutsche Forschungsgemeinschaft through SFB 616 "Energy Dissipation at Surfaces" is gratefully acknowledged.

*Corresponding author.
†gr.jnawali@uni-due.de
‡Present address: Johannes Kepler University Linz, Institute of Experimental Physics, Altenberger Str. 69, A-4040 Linz, Austria; thorsten.wagner@jku.at

[1] F. Y. Yang, K. Liu, K. Hong, D. H. Reich, P. C. Searson, and C. L. Chien, Science **284**, 1335 (1999).
[2] Yu. M. Koroteev, G. Bihlmayer, J. E. Gayone, E. V. Chulkov, S. Blügel, P. M. Echenique, and Ph. Hofmann, Phys. Rev. Lett. **93**, 046403 (2004).
[3] Ph. Hofmann, Prog. Surf. Sci. **81**, 191 (2006).
[4] T. Hirahara, T. Nagao, I. Matsuda, G. Bihlmayer, E. V. Chulkov, Yu. M. Koroteev, P. M. Echenique, M. Saito, and S. Hasegawa, Phys. Rev. Lett. **97**, 146803 (2006).
[5] T. Hirahara, I. Matsuda, S. Yamazaki, N. Miyata, S. Hasegawa, and T. Nagao, Appl. Phys. Lett. **91**, 202106 (2007).
[6] T. Hirahara, K. Miyamoto, I. Matsuda, T. Kadono, A. Kimura, T. Nagao, G. Bihlmayer, E. V. Chulkov, S. Qiao, K. Shimada, H. Namatame, M. Taniguchi, and S. Hasegawa, Phys. Rev. B **76**, 153305 (2007).
[7] N. Garcia, Y. H. Kao, and M. Strongin, Phys. Rev. B **5**, 2029 (1972).
[8] G. Jnawali, H. Hattab, C. A. Bobisch, A. Bernhart, E. Zubkov, R. Möller, and M. Horn-von Hoegen, Phys. Rev. B **78**, 035321 (2008).
[9] G. Jnawali, H. Hattab, B. Krenzer, and M. Horn von Hoegen, Phys. Rev. B **74**, 195340 (2006).
[10] T. Nagao, J. T. Sadowski, M. Saito, S. Yaginuma, Y. Fujikawa, T. Kogure, T. Ohno, Y. Hasegawa, S. Hasegawa, and T. Sakurai, Phys. Rev. Lett. **93**, 105501 (2004).
[11] J. T. Sadowski, T. Nagao, S. Yaginuma, Y. Fujikawa, A. Al-Mahboob, K. Nakajima, T. Sakurai, G. E. Thayer, and R. M. Tromp, Appl. Phys. Lett. **86**, 073109 (2005).
[12] Z. Zhang and M. G. Lagally, Science **276**, 377 (1997).
[13] M. Kammler and M. Horn-von Hoegen, Surf. Sci. **576**, 56 (2005).
[14] H. Hattab, G. Jnawali, C. A. Bobisch, A. Bernhart, E. Zubkov, R. Möller, and M. Horn-von Hoegen (unpublished).
[15] R. Gomer, Rep. Prog. Phys. **53**, 917 (1990).
[16] K. Oura, V. G. Lifshits, A. A. Saranin, A. V. Zotov, and M. Katayama, *Surface Science: An Introduction* (Springer-Verlag, Berlin, 2003).
[17] J. A. Venables, Philos. Mag. **27**, 697 (1973).
[18] J. A. Venables, G. D. T. Spiller, and M. Hanbücken, Rep. Prog. Phys. **47**, 399 (1984).
[19] Y.-W. Mo, J. Kleiner, M. B. Webb, and M. G. Lagally, Surf. Sci. **268**, 275 (1992).
[20] Y. W. Mo, J. Kleiner, M. B. Webb, and M. G. Lagally, Phys. Rev. Lett. **66**, 1998 (1991).
[21] R. E. MacFarlane, *The Physics of Semimetals and Narrow Gap Semiconductors* (Pergamon, New York, 1971).
[22] H. Brune, H. Röder, C. Boragno, and K. Kern, Phys. Rev. Lett. **73**, 1955 (1994).
[23] T. A. Witten and L. M. Sander, Phys. Rev. B **27**, 5686 (1983).
[24] H. Brune, Ch. Romainczyk, H. Röder, and K. Kern, Nature (London) **369**, 469 (1994).
[25] T. Michely and J. Krug, *Islands, Mounds and Atoms*, Springer Series in Surface Sciences (Springer-Verlag, Berlin, 2004).